J. exp. Biol. **127**, 59–78 (1987)
Printed in Great Britain © *The Company of Biologists Limited 1987*

THE WAKE OF A KESTREL (*FALCO TINNUNCULUS*) IN FLAPPING FLIGHT

BY G. R. SPEDDING*

Department of Zoology, University of Bristol, Woodland Road, Bristol BS8 1UG

Accepted 19 August 1986

SUMMARY

The structure of the wake behind a kestrel in medium-speed flight down a 36 m length of corridor was analysed qualitatively and quantitatively by stereophotogrammetry of multiple flash photographs of the motion of small soap-covered helium bubbles. The wake consists of a pair of continuous, undulating trailing vortices. The upstroke is therefore aerodynamically active and the circulation appears to remain constant along the wing whose geometry is altered during the course of the wingstroke. It is argued that the flight kinematics, and so the wake structure, of the kestrel may be typical of flapping flight at medium speeds and a flight model based on this wake geometry is presented. Rough estimates of the rate of momentum generated in the wake balance the weight almost exactly and a direct estimate of the induced power requirement from the wake measurements is obtained. The significance of these results for the various alternative aerodynamic descriptions and energetic predictions of models of flapping animal flight is briefly assessed.

INTRODUCTION

Previous investigations have demonstrated the existence of vortex rings in the wake of birds flying slowly down the length of an 8 m flight cage (Spedding, Rayner & Pennycuick, 1984; Spedding, 1986) although some doubts as to the adequacy of this description were raised by the apparent shortfall in the momentum measured in this wake compared with that required for weight support. While these conditions provided a stern test of the flight model under investigation (Rayner, 1979*a*,*b*), where a high degree of unsteadiness in the flow necessitates an accurate aerodynamic model in order to estimate the induced power requirement, it is perhaps of more interest to a practical ecologist to obtain information about flight at the higher speeds commonly used by most birds in migrating or commuting flights. The significance of two characteristic flight speeds, the minimum power speed, U_{mp}, and the maximum range speed, U_{mr}, was identified by Pennycuick (1968), derived from the U-shaped P(U) curves predicted by his actuator-disk flight model (P is the power required to fly, U is the flight speed). These characteristic speeds persist in the vortex ring model

* Present address: Department of Aerospace Engineering, University of Southern California, University Park, Los Angeles, CA 90089–0192, USA.

Key words: flight, wake, kestrel.

calculations (Rayner, 1979*b*) and, while the parasite and profile power requirements consume a greater fraction of the total power, the induced power contribution remains significant at these flight speeds.

Although there are well-documented differences in the wing beat kinematics of birds flying at low and high speeds (e.g. Brown, 1953, 1963) no flight model explicitly accounts for the different flight styles which may occur. In the flow visualization experiments which have been performed thus far, vortex rings have been described in the wake of small passerines (Kokshaysky, 1979) and for a pigeon and a jackdaw (Spedding *et al.* 1984; Spedding, 1986) in slow flight, all in flight cages or tanks. It might reasonably be expected that the lower wing beat amplitudes and accelerations more typical of cruising flight at higher flight speeds would significantly alter the distribution of wake vorticity. At the same time, at these lower reduced frequencies (the reduced frequency, $\Omega = c\omega/2U$, where c is the wing chord, ω is the radian frequency and U the mean forward velocity), it may be possible to considerably simplify some of the assumptions required in the aerodynamic analysis.

In the previous paper (Spedding, 1987), the steady gliding flight of a kestrel was found to accord well with classical steady-state aerodynamic theory. Here the wake of the same kestrel under identical conditions, but in flapping flight, will be investigated to determine the extent to which these properties remain in the domain of small but finite reduced frequency.

MATERIALS AND METHODS

Generally, the apparatus and methods are identical to those described in Spedding (1987), the only difference being the flight behaviour of the kestrel as it grew more accustomed to the experimental conditions and operator 2 was positioned slightly further away from the cameras to encourage flapping flight through the bubbles. The flight path is shown schematically in Fig. 1. After an initial drop from take-off at point 1, the bird would fly level at 400–450 mm from the floor down the length of the corridor before pulling up and alighting on point 2. The take-off and landing points were about 1 m in height. Six of these flights were timed with a stopwatch, recording a mean ground speed of $6\ m\ s^{-1}$ from point 1 to point 2. Accounting for acceleration and deceleration at either end of the flight, the ground speed in mid-flight was estimated to be around $7\ m\ s^{-1}$, in agreement with that calculated from the horizontal distance between successive tail images on the stereophotographs.

Two stereopairs were digitized and reconstructed as three-dimensional velocity fields, following previously established procedures (Spedding *et al.* 1984). Series of two-dimensional slices were taken through these data, and velocity profiles were recorded in the plane of the sections. The coordinate system is a right-handed one, with the origin at the intersection of the left camera lens principal axis with the back wall. The Z axis is coincident with the lens principal axis, X runs from left to right, parallel to the line of flight, and vertical distances are measured in Y (see fig. 2 of Spedding, 1987).

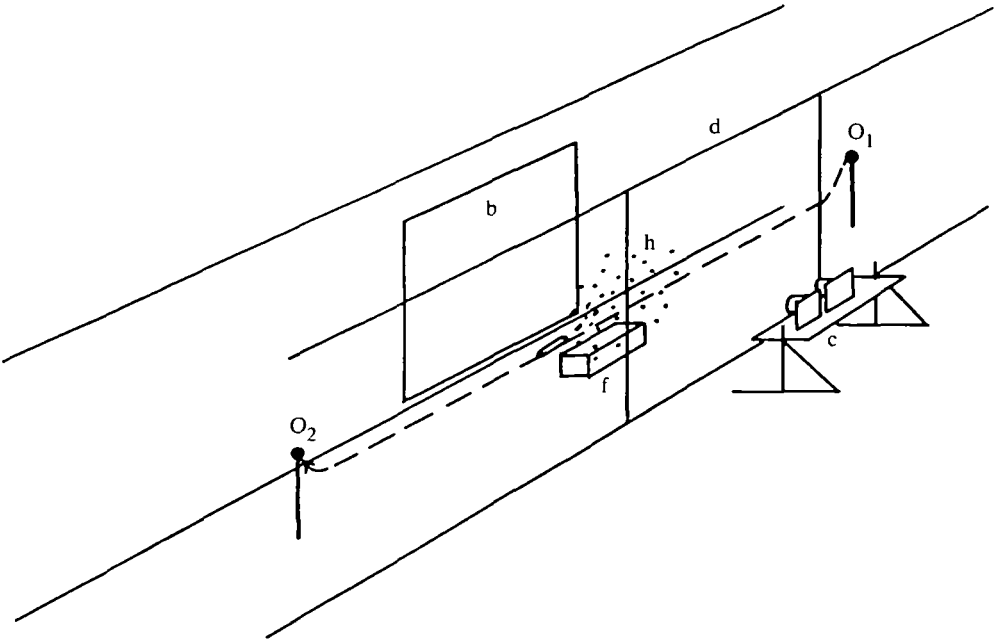

Fig. 1. Diagram of the apparatus schematic as in Spedding (1987), but showing the flight path taken by the kestrel in flapping flight experiments. The average flying height (425 mm) was slightly above that recorded in gliding flights. The symbols are defined in the caption to fig. 1 in Spedding (1987).

RESULTS

Qualitative results

At these flight speeds, the wavelength of the wake (the horizontal distance between wake elements formed by two consecutive instances of a particular point in the wing beat cycle) is longer than could usually be covered by the cloud of helium bubbles, and the structure of the wake must be deduced from more than one stereopair.

Figs 2 and 3 are two stereopairs showing partial coverage of the vortex wake behind a kestrel in flapping flight. In Fig. 2, the bird, flying from right to left, is near the end of an upstroke during which the primary feathers have been flexed and inclined downstream of the mean flow. In the last of the four kestrel images, the primaries are being re-extended out into the flow. The bubbles mark the flow of the previous downstroke and the beginning of the upstroke, and are situated mainly in the background so as to visualize the wake behind the starboard wing. Behind a central induced downward flow, a curved vortex core is visible, marked by an axial flow along the core and a circulatory flow around it. The axial flow is towards the wingtip and is therefore a viscous drag wake. The vortex core can be clearly seen continuing along a straight cylindrical component of the wake, produced during the upstroke. The continuity between these two sections is unambiguously shown by the axial core flow, and Fig. 3 shows the upstroke portion of the wake as a straight cylindrical vortex of larger diameter than that produced by the downstroke. Here,

bubble tracks show the foreground wake shed by the port wing. The principal features of the wake are visible in Fig. 4 which shows, from right to left, a linear vortex core of large diameter shed during an upstroke, a curved, smaller diameter core produced by the following downstroke with the flow induced by this vortex clearly visible towards the centre of the wake, and finally, a continuation of this vortex core into the next upstroke as demonstrated by the axial flow along the core. At their lowest extent the wake trailing vortices are about 250 mm from the ground. The propensity for bubbles to become trapped inside a vortex and move axially along its length was found to be quite convenient for tracing the core location and Fig. 5 shows the wingtip trailing vortex behind the starboard wing during the first half of a downstroke marked in this way. In this photograph, the continuity between upstroke and downstroke wake vortices is clearly visible.

In all stereopairs examined, the observed wake structure was consistent with a continuous undulating vortex pair without detectable concentrations of transverse, or cross-stream vorticity joining the two cores. If transverse lines of vorticity are present, then they are not aggregated into recognizable vortex structures. Fig. 6 is a

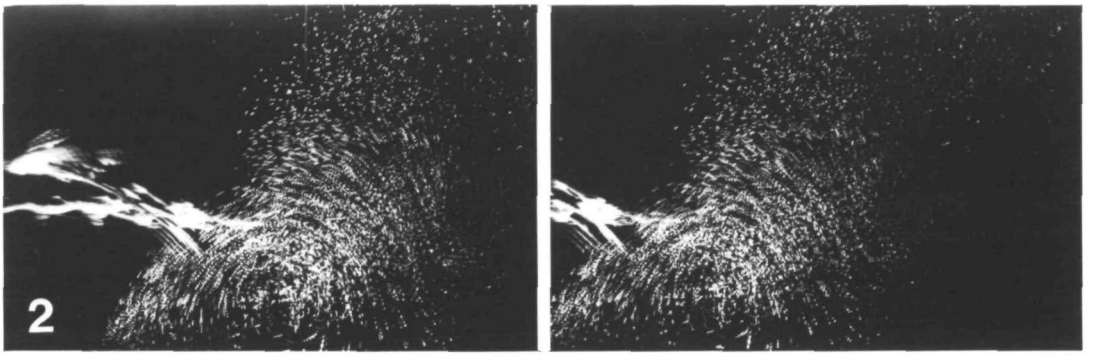

Fig. 2. Stereopair of the vortex wake behind a kestrel in medium-speed flight. The direction of flight was from right to left and the flexed primary feathers can be distinguished during the upstroke. The mean time between successive flashes was 16 ms.

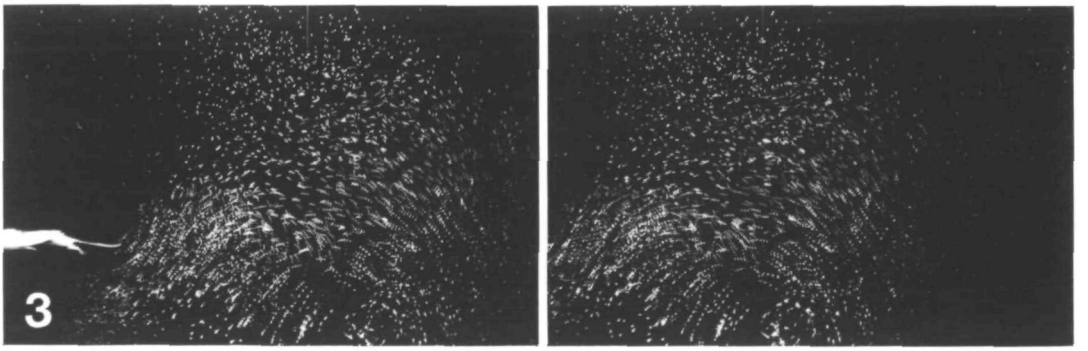

Fig. 3. As Fig. 2, but the most clearly visible wake structure is a straight line vortex, apparently shed from the end of the secondary feathers or the folded primary feathers during the upstroke. Mean time between flashes was 16 ms.

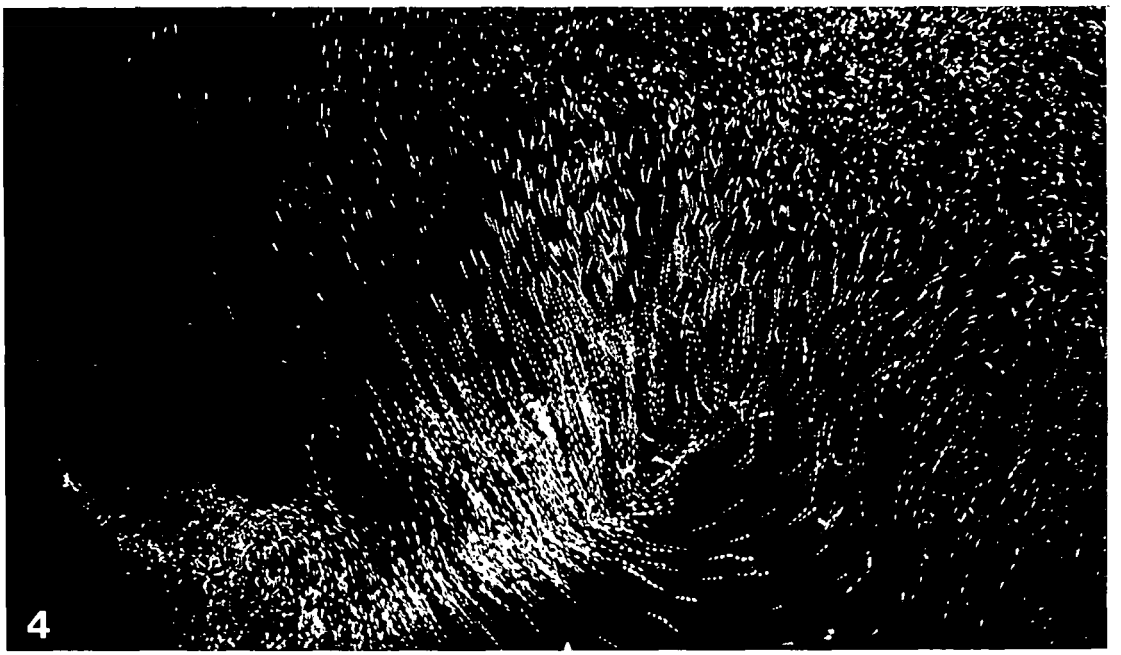

Fig. 4. Single photograph (the left one of a pair) covering approximately one period of the wing beat cycle, visualized by bubbles mainly in the background of the flow field. The upstroke and downstroke core structures may be recognized from Figs 2 and 3 and the continuity of the trailing vortex into the upstroke is clear from the viscous wake visualized by bubbles moving axially along the core and towards the bird (flight was again from right to left). Mean flash interval was 12·5 ms.

diagram of the wake as judged by qualitative inspection of all stereopairs of the wake. The fitness of such a description of the wake may be tested with some simple quantitative wake measurements.

Quantitative results

The three-dimensional velocity field was calculated from a full stereophotogrammetric analysis of two of the kestrel flights. Examples of the reconstructed bubble field in one of these are shown in Figs 7 and 8, which are elevation and plan views of the wake produced by half a downstroke followed by half an upstroke. Bubbles are confined to the foreground in this case and the wake is assumed to be symmetrical about the vertical plane along the line of flight. The line of flight is an average estimate from all stereopairs and the standard deviation in Z is ± 50 mm. This corresponds to less than 0·15 of the wing semispan, b. Fig. 8 also shows the location of numbered and lettered sections taken vertically across (spanwise) and along (streamwise) the length of the wake, respectively.

If, as postulated in the previous section, the trailing vortices in the wake are continuous and not connected by vortex lines running transversely across the wake, then according to laws of vorticity established for inviscid incompressible fluids by Helmholtz and Kelvin (as outlined, for example, by Batchelor, 1967), the circulation

around each vortex must be invariant along its length. Accordingly, the circulations measured by integration around the edge of the vortex core should be equal at all downstream core cross-sections. Figs 9 and 10 show the $w(Y)$ velocity distributions in two cross-sections taken across the mid-sections of the downstroke and upstroke wake vortices (sections 8 and 3 of Fig. 8). The curves have been drawn by eye to account for the finite thickness of the transects in Z and the width of the core may be

Fig. 5. The location of the downstroke trailing vortex is marked by axial flow along the core. Careful inspection of this photograph shows the connection between upstroke and downstroke trailing vortices. A starting vortex connecting the two sides of the wake would be here, if present, but was observed in none of the wake photographs. Mean flash interval was 16 ms.

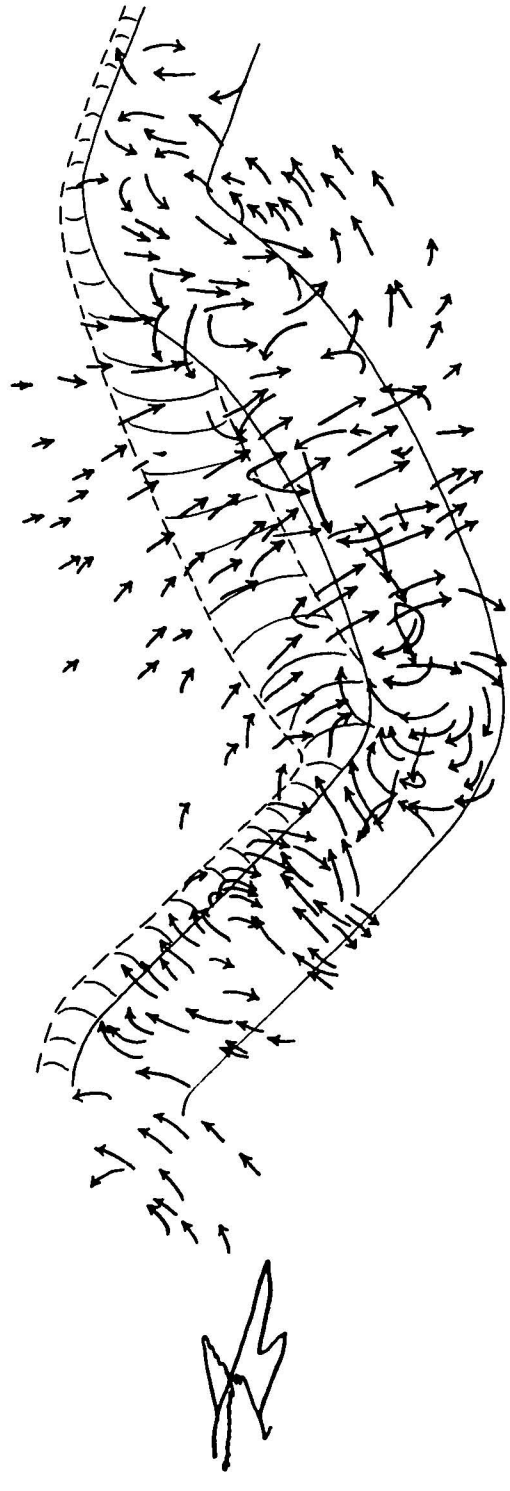

Fig. 6. Schematic representation of the wake as reconstructed from stereophotographs. The arrows represent the three-dimensional velocity vectors (or rather their projection onto the XY plane of the paper) in the neighbourhood of the foreground vortex, whose counterpart behind the starboard wing is indicated by dashed lines. The location of the bird with respect to the wake vortices suggests that either the wing beat amplitude is not symmetrical about the wing root, or the wake has convected downwards since being shed at the wingtips, or both.

estimated from the distance between w_{max} and w_{min}. If the vortex core is assumed to be circular and to contain all the vorticity then the vortex has circulation Γ,

$$\Gamma = 2\pi r w_t, \quad (1)$$

where r is the core radius and w_t is the tangential velocity at the core edge. From Figs 9 and 10, the downstroke circulation, $\Gamma_1 = 0{\cdot}50\,m^2\,s^{-1}$ and the upstroke circulation, $\Gamma_2 = 0{\cdot}60\,m^2\,s^{-1}$. Results from other wake cross-sections were quite consistent with this result. The difference between these two values is smaller than the uncertainty in their calculation and it is concluded that there is no significant component of spanwise vorticity in the wake.

DISCUSSION

Wing beat kinematics and wake structure

The circulation measurements reported above support the notion that the wake of a flapping kestrel is composed of a continuous vortex pair of constant circulation without significant components of cross-stream vorticity connecting the two. The wake structure is thus quite different from that reported for small passerines (Kokshaysky, 1979) or for the slow flight of the pigeon or jackdaw (Spedding *et al.* 1984; Spedding, 1986). In those cases where vortex rings are produced in the wake,

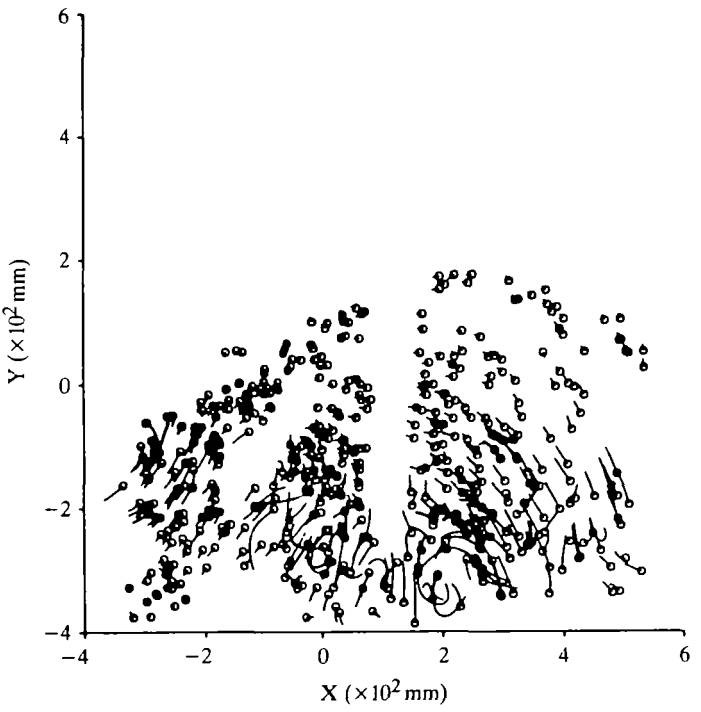

Fig. 7. Side view of a bubble field reconstructed from stereophotographs. The leading bubble is denoted by a circle and the length of the trailing tail is proportional to its velocity in XY.

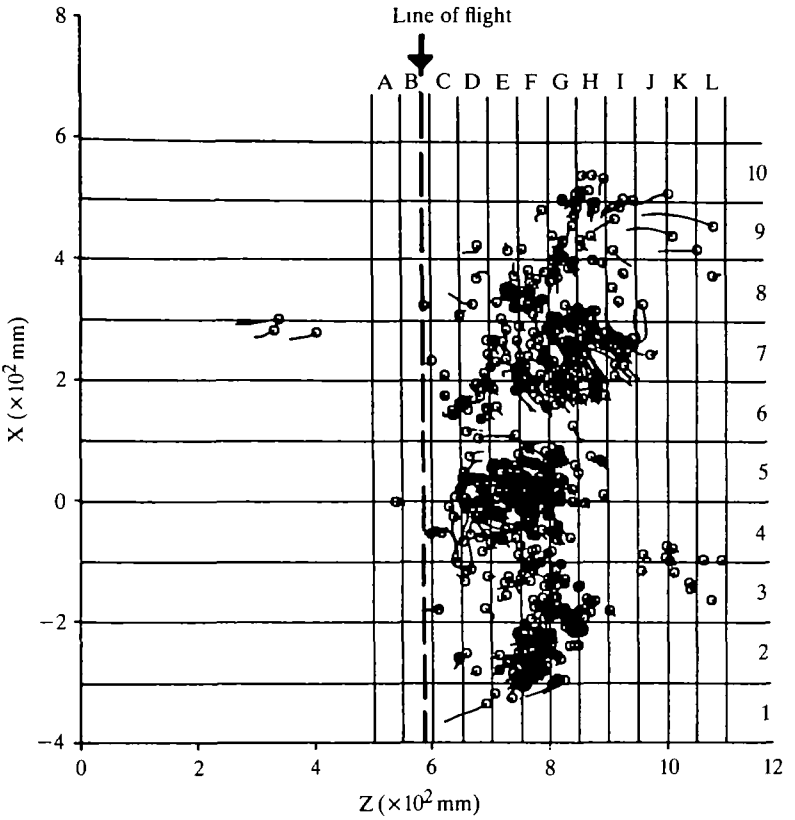

Fig. 8. The same bubble field as in Fig. 7, but viewed from above. Numbered and lettered sections denote the location of serial sections taken across and along the wake.

the rapid acceleration and deceleration of the wings at the beginning and end of the downstroke alters the circulation on the wing with the concomitant shedding of vorticity into the wake, and the trailing vortex lines are closed up into a loop by these starting and stopping vortices. In the medium-speed flight of the kestrel, these rapid accelerations of the wings are absent, as are the cross-stream vortices. There *is* transverse vorticity (a Z-component) in the wake of course, manifested in the outward curvature of the downstroke trailing vortex (in the Z direction) when it is not parallel to the X axis.

During the upstroke of the kestrel, the wings are not folded close to the body, but the primary feathers are flexed and closed up, parallel to the incident air flow, while the secondary feathers remain extended into the flow. The secondary feathers remain loaded and perform aerodynamic work during the upstroke, as confirmed by the presence of trailing vortices in the wake during this period. Moreover, the circulation around the secondary feathers appears to be maintained at a constant level and the wing beat can be conceived as a cycle of loading and unloading of the primary feathers as they are extended on the downstroke and flexed during the upstroke.

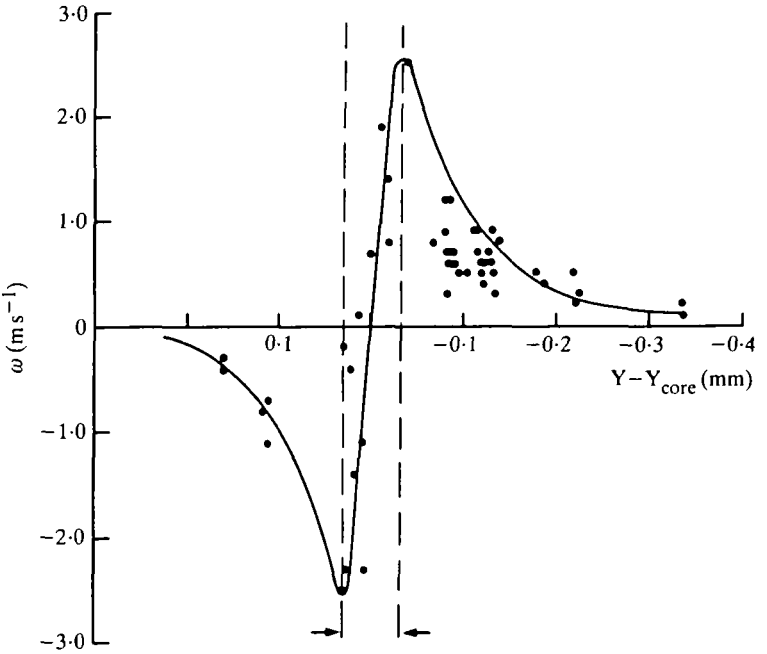

Fig. 9. w(Y) for a section through the downstroke vortex core. The core diameter was estimated from the distance between the two broken lines.

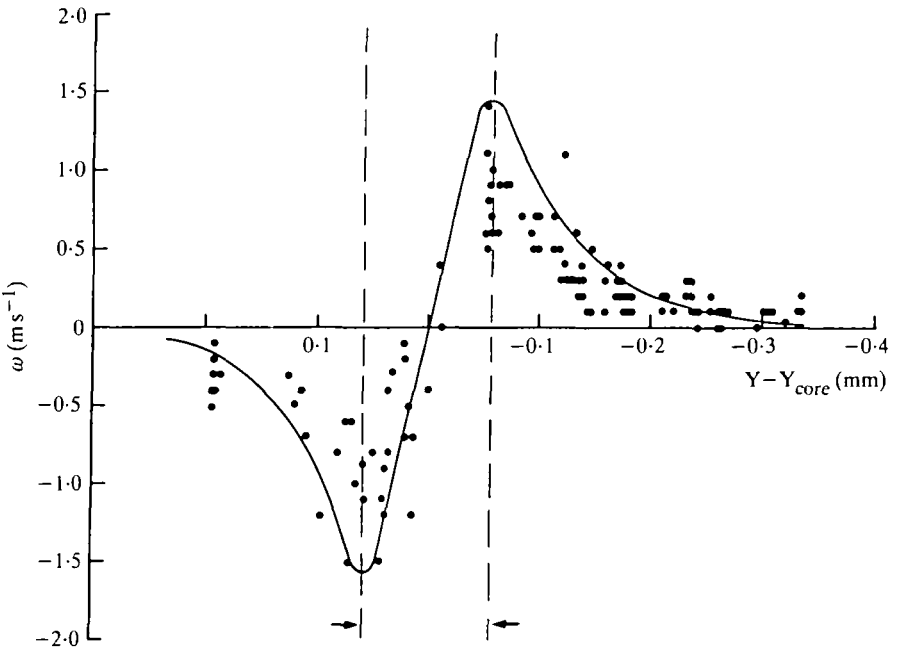

Fig. 10. w(Y) for a section through the upstroke vortex core. w at the edge of the core is lower than for the downstroke vortex but the core diameter is larger.

During the upstroke, the folding of the primary feathers appears to be such that the trailing vortex is shed from the end of the secondary feathers, or around the flexed primaries. This shift in location of the shedding point is consistent with the experimental results of McCormick & Padakannaya (1971) showing that the effect of a drooped wingtip is to increase the strength of the inner trailing vorticity at the hinge, causing the wingtip trailing vortex to move inboard towards the hinge.

These results also support the careful observations of Brown (1953, 1963) who deduced from high-speed cinematography of birds in medium-speed flight that the secondary feathers provide aerodynamic lift during the upstroke. The flight speed and wing beat kinematics of the kestrel in this study appear to be similar to those of free-flying kestrels as recorded by high-speed ciné film (Scholey, 1983) and are quite

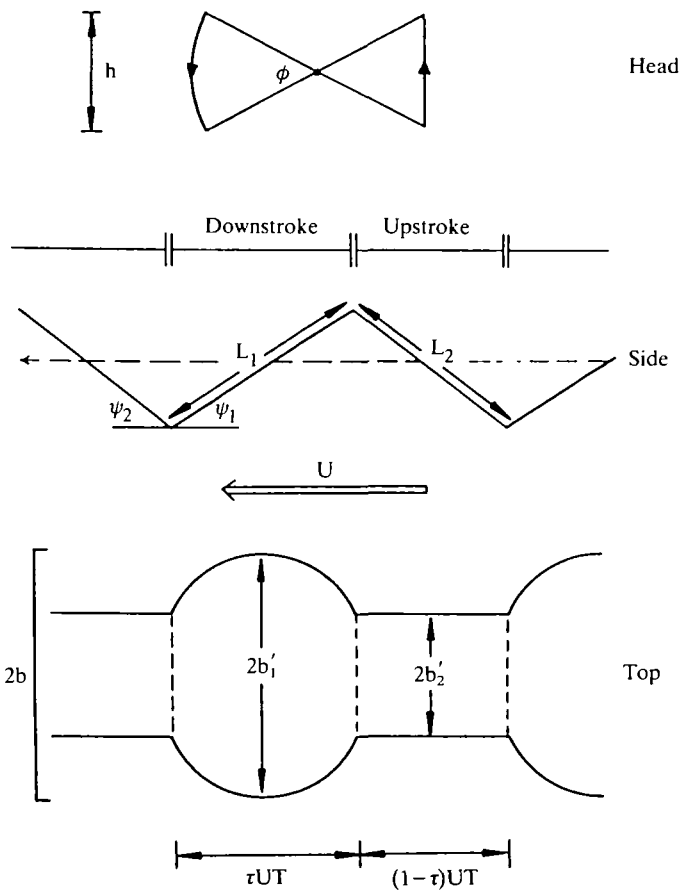

Fig. 11. Diagram of the vortex wake of a kestrel which also forms the basis for the general model of medium-speed flapping flight. The dashed lines across the wake indicate the location where weak transverse vortices might appear at slightly lower flight speeds, or during periods of acceleration. h, wake amplitude; b, wing semispan; ϕ, stroke amplitude; ψ_1, ψ_2, wake inclination for the downstroke and upstroke, respectively; U, flight speed; T, stroke period; τ, downstroke ratio.

characteristic of the low-amplitude wing beat cruising flight of many species (Brown, 1953, 1963). This being the case, there is no reason to suspect that the resulting wake structures would be substantially different either, and it is proposed that the continuous undulating vortex pair wake structure, described here for the kestrel, is the usual pattern in this type of flight.

Flapping flight with constant circulation

The fact that this wake pattern has a simple geometric description with a constant value of the circulation around the trailing vortex lines allows an aerodynamic analysis to proceed with several simplifications. The way in which such an analysis might be conducted is outlined in the following section.

Consider a bird which flies in steady horizontal flight at speed U, flapping its wings with a frequency f, through an angle, ϕ, the wing beat amplitude (Fig. 11). The wingspan is 2b and the wing beat is such that the wing is fully extended on the downstroke but is gradually flexed and then re-extended during the upstroke so that, at mid-stroke, the effective wingspan is the distance between the ends of the secondary feathers in addition to the small spanwise extent of the flexed primary feathers. Let this distance be denoted $2b_2$. The result of this upstroke is assumed to leave a straight section of wake behind, as measured in the kestrel wake, of spanwise extent $R'2b_2$. R′ is a dimensionless wake spacing, which was measured to be 0·76 in Spedding (1987) for steady-state gliding, close to the value of 0·785 for an elliptically loaded wingpair. In the absence of a direct experimental measurement, either value could be used, although somewhat higher R′ values of 0·85–0·95 were measured in the wake in flapping flight. A compromise choice to reflect this higher possibility might be 0·85, pending further experimental evidence. Similarly, the greatest spanwise extent of the wake produced on the downstroke is R′2b. For convenience, I define:

$$2b_1' = R'2b,$$

$$2b_2' = R'2b_2,$$

and

$$B = 2b_1' - 2b_2'. \tag{2}$$

The wavelength of the wake is UT, where $T = 1/f$ is the stroke period, and if τ, the downstroke ratio, is the fraction of T spent on the downstroke, the angles ψ_1 and ψ_2 are given by

$$\psi_1 = \tan^{-1}[h/(\tau UT)]$$

and

$$\psi_2 = \tan^{-1}\{h/[(1-\tau)UT]\}, \tag{3}$$

where

$$h = 2b_1' \tan(\phi/2). \tag{4}$$

The lengths L_1 and L_2 (Fig. 11) may be written

$$L_1 = [h^2 + (\tau UT)^2]^{1/2}$$

and

$$L_2 = \{h^2 + [(1-\tau)UT]^2\}^{1/2}. \tag{5}$$

The planar areas A_1 and A_2 of the downstroke and upstroke wakes are

$$A_1 = 2b_2' \cdot L_1 + 2\left\{\left[\tan^{-1}\left(\frac{2Bl}{l^2 - B^2}\right)\right]\left[\frac{l^2 + B^2}{2B}\right]^2 - l\left[\left(\frac{l^2 + B^2}{2B}\right)^2 - l^2\right]^{1/2}\right\},$$

and

$$A_2 = 2b_2' \cdot L_2, \tag{6}$$

where $2l = L_1$, and the expression for A_1 assumes that a circular arc, of maximum spanwise extent $2b_1'$ on the downstroke, joins the straight line upstroke wake segments. Now, the momentum normal to the plane of each wake segment can be written

$$\mathbf{Q}_1 = \rho\Gamma A_1$$

and

$$\mathbf{Q}_2 = \rho\Gamma A_2. \tag{7}$$

The sum of the momenta represented by the horizontal projection of areas 1 and 2 on to XZ must balance the weight of the bird minus the contributions due to the vertical components of the profile and parasite drags, $\mathbf{D}_{pro}$ and $\mathbf{D}_{par}$ for one wing beat period, T. Similarly, the rate of change of the horizontal component of momentum, given by the sum of the vertical projected areas of A_1 and A_2 (A_2 contributes a drag) times $\rho\Gamma/T$ must balance the drag on the bird. In general form,

$$|\mathbf{Q}_1|(\mathbf{j}\cos\psi_1 - \mathbf{i}\sin\psi_1) + |\mathbf{Q}_2|(\mathbf{j}\cos\psi_2 + \mathbf{i}\sin\psi_2) = T(M\boldsymbol{g}\mathbf{j} - \mathbf{D}_{par} - \mathbf{D}_{pro}), \tag{8}$$

where $\boldsymbol{g}$ is the acceleration due to gravity, M is the mass of the bird and $\mathbf{i}$ and $\mathbf{j}$ are unit vectors along the X and Y axes, respectively.

Equation 8 states that the wake momentum must balance the vector sum of the bird's weight together with the parasite and profile drags for the time T and is seen to be simply a recasting of equation 24 of Rayner (1979*a*) appropriate for this wake. Resolving this into the lift and drag force components (time averaged over T) normal and parallel to the direction of flight,

$$L = \rho\Gamma(A_1\cos\psi_1 + A_2\cos\psi_2)/T = (M\boldsymbol{g} - \mathbf{D}_{pro}\sin\alpha_1 - \mathbf{D}_{par}\sin\alpha_2) \tag{9}$$

$$D = \rho\Gamma(A_1\sin\psi_1 - A_2\sin\psi_2)/T. \tag{10}$$

D in equation 10 is the vector sum of the horizontal components of the profile and parasite drags,

$$D = \mathbf{D}_{pro}\cos\alpha_1 + \mathbf{D}_{par}\cos\alpha_2. \tag{11}$$

The angles α_1 and α_2 depend on angle of the body to the horizontal and the inclination of the stroke plane. In this mode of flight, α_2 may be assumed to be small, equivalent to ignoring the lift component of the parasite drag on the body. If T is specified, α_2 is given by ψ_1 and U. Alternatively, some reasonable value may be assigned for a limited range of moderate flight speeds. The calculation of $\mathbf{D}_{pro}$ itself is fraught with difficulties and uncertainty. It is caused by skin friction and the resultant viscous losses in the boundary layer which separates before the trailing edge. The resulting wake exerts a pressure drag force on the aerofoil, and this is the

wake which can be seen in Figs 4 and 5. The magnitude of $\mathbf{D}_{pro}$ depends on the shape and smoothness of the surface of the aerofoil, the condition of the boundary layer, and the flow Reynolds number. Rather than become enmeshed in the intricacies of this subject, suffice to note that $\mathbf{D}_{pro}$ is usually estimated from some form of

$$\mathbf{D}_{pro} = \tfrac{1}{2}\rho S U^2 C_{D,pro}, \tag{12}$$

where S is the wing area, U is the incident velocity on the aerofoil, and $C_{D,pro}$ is calculated or measured by experiment. Both Rayner (1979*a*) and Ellington (1984) have discussed this issue in some depth in the context of animal flight. It should be further noted that, for the wingstroke described here, S varies during the course of the wing beat cycle, and the calculation of $\mathbf{D}_{pro}$ should take this into account.

Similarly, the parasite drag, $\mathbf{D}_{par}$ can be written

$$\mathbf{D}_{par} = \tfrac{1}{2}\rho A U^2, \tag{13}$$

where A is the equivalent flat plate area presented by the body to the freestream velocity U, and details of its calculation need not be of further concern in this discussion.

Parameterization of the model

After a straightforward consideration of the wake geometry and enforcing the equilibrium condition of force balance on the bird, equations 9 and 10 may be solved for Γ and one other unknown wing beat kinematic parameter. If ϕ and T are given, together with the wing shape as expressed by 2b and $2b_2$, then the remaining unknown is the stroke period τ, which must take on a value such that the momenta represented by areas A_1 and A_2 satisfy equations 9 and 10. This is not the sole possible choice of governing parameters however, and equations 9 and 10 could equally well be solved for the wing beat amplitude ϕ, given a reasonable value of τ. Note also that the formulation of a solvable model does not depend on a particularly rigid adherence to the exact geometry of Fig. 11. It is obvious from even the most casual of observations of birds in cruising flight, that the degree of flexure, or sweep, of the primary feathers, during both upstroke and downstroke, varies widely according to species and according to flight speed, and this can be readily incorporated *via* a judicious selection of 2b and $2b_2$. Similarly, a curved upstroke wake geometry could be written into equation 6 for A_2.

It is interesting to note how the *shape* of the wing is accounted for directly in the differing geometries of the downstroke and upstroke wakes, due to this folding of the wing back to the secondary feathers during the upstroke. This is reflected in the relative magnitudes of the thrust and lift components of the wake which must satisfy equation 8 overall. A parametric analysis along these lines might use b_2/b as a controlling parameter.

Calculation of the induced power

Given that the circulation of the wake vortices, and hence, the circulation on the wing, remain constant, or at least fluctuate only little, the transverse vorticity in the

wake must therefore be weak, as concluded from the experimental results, and the induced drag can be quickly derived from a quasi-steady aerodynamic analysis. This is quite consistent with the low values of the reduced frequency $\Omega \approx 0{\cdot}2$. Elementary results from lifting line theory may therefore be applied where the wing is replaced by a lifting line at the trailing edge which is assumed to be straight and normal to the flow, and all trailing vortices leave the trailing edge in lines parallel to the direction of motion. The assumption of a planar near wake is not affected by subsequent roll-up of the wake vortices further downstream. Moreover, extrapolating from the results of the gliding experiment reported in Spedding (1987), it seems reasonable to assume that the spanwise circulation distribution on the wing differs little from the elliptical loading commonly assumed in classical aerodynamics, and one immediately arrives at an expression for the induced drag, $D_i = \mathbf{i}\mathbf{D}_i$ (Milne-Thompson, 1966, p. 203)

$$D_i = \tfrac{1}{8}\pi\rho\Gamma_o^2, \tag{14}$$

where Γ_o is the circulation at the centre line, which is equal to the circulation of the vortices in the wake, Γ. Now the induced power is the work done against induced drag, equivalent to rate of increase of wake kinetic energy per unit time, and is just

$$P_i = D_i \cdot U. \tag{15}$$

The simple wake model with constant circulation of wake vortices and the neglect of unsteady terms enables this analysis to be conducted without unduly lengthy or complex computations, although these assumptions necessarily limit the scope of the analysis to cruising flight of the type described for the kestrel.

Momentum balance and induced power requirement

In view of the wake momentum deficits measured in experiments involving the pigeon and the jackdaw in slow flight (Spedding *et al.* 1984; Spedding, 1986), it is of some interest to perform a rough check on the wake momentum in the case of the cruising flight of the kestrel. If one assumes, for the moment, that the vertical components of the parasite and profile drags are small, then equation 9 reduces to

$$\rho\Gamma(A_1\cos\psi_1 + A_2\cos\psi_2)/T = M\boldsymbol{g}. \tag{16}$$

Table 1 summarizes the wing beat kinematic data for the kestrel, together with some parameters describing the wake geometry. All quantities are known or are calculable on the left-hand side of equation 16, which evaluates to 2·15 N. This compares with the bird's weight, $M\boldsymbol{g} = 2{\cdot}06$ N; the rate of generation of the vertical component of the wake momentum almost exactly balances the weight. This result further implies that the contributions to weight support from the parasite and profile drags are small. The inclination of the body axis to the horizontal is small so the $\mathbf{D}_{par}$ contribution is low, and the wing does aerodynamic work on both the downstroke and the upstroke so the net vertical $\mathbf{D}_{pro}$ force over one wing stroke will be correspondingly diminished. It is therefore with some justification then that we now neglect both and proceed onward to calculate the induced drag on the wings from equation 14. Substituting the mean value of $\bar{\Gamma} = 0{\cdot}55$, $D_i = 0{\cdot}14$ N. Now the

Table 1. *Morphological, kinematic and wake geometric data for the kestrel in cruising flight*

	Symbol	Units	Quantity
Body mass	M	kg	0·210
Wing semispan	b	m	0·338
Wing area	S	m^2	0·052
Mean chord	c	m	0·076
Stroke period*	T	s	0·13
Stroke amplitude*	ϕ	rad	0·89
Flight speed	U	$m\,s^{-1}$	7·0
Downstroke ratio*	τ		0·55
Reduced frequency	$\Omega = c\omega/2U$		0·27
Chord Reynolds no.†	$Re_c = Uc/\nu$		$3{\cdot}5\times10^4$
Wake amplitude	h	m	0·32
Wake inclination	ψ_1	rad	0·58
	ψ_2	rad	0·66
Wake spacing	b_1'	m	0·33
	b_2'	m	0·17
	$R_1' = b_1'/b$		0·98
	$R_2' = b_2'/b$		0·50
Core radius	r_1	m	0·032
	r_2	m	0·066
	$r_1' = r_1/b_1'$		0·097
	$r_2' = r_2/b_2'$		0·391
Planar wake area	A_1	m^2	0·33
	A_2	m^2	0·17
Vortex circulation	Γ_1	$m^2\,s^{-1}$	0·50
	Γ_2	$m^2\,s^{-1}$	0·60
	$\bar{\Gamma} = (\Gamma_1+\Gamma_2)/2$	$m^2\,s^{-1}$	0·55

* Kinematic parameters marked with asterisk were calculated from wake measurements.
† ν is the kinematic viscosity of the fluid.
Subscripts 1 and 2 refer to the downstroke and upstroke, respectively.

induced power can be calculated directly from equation 15 and $P_i = 1{\cdot}0\,W$. For comparison, the induced power requirement from actuator disk theory may be written (Pennycuick, 1975)

$$P_i = kW^2/2\rho US_d, \tag{17}$$

where $S_d = \pi b^2$ is the wing disk area, $W = M\boldsymbol{g}$ is the weight, and the factor $k \geqslant 1$, which is included to account for unsteady wake energy losses and is usually set at around 1·2. Calculated from equation 17, $P_i = 0{\cdot}84\,W$. The agreement between the two estimates is good, and the slightly higher value measured directly from the wake analysis may reflect the more realistic wake geometry upon which it is based. The consistency of these approximate numerical calculations lends some support to the flight model formulation outlined in the previous section.

Ground effect

In Spedding (1987), equation 10 was used to estimate the magnitude of ground effect in gliding flight and it was concluded that ground effect was of limited

importance at flying height, h, of the order of the semispan, b, but that its effect in reduction of $\mathbf{D}_i$ would increase rapidly as h approaches the mean chord c. The calculation is not so straightforward in the unsteady case and one can only speculate as to the possible effects on this wake. The lowest extent of the trailing vortex core in the wakes which provided material for the quantitative analyses was about 280 mm, or about six mean core radii from ground level. This is about 3·7 mean chord lengths, when a 25 % reduction in $\mathbf{D}_i$ would be expected in steady horizontal flight at this altitude. The effect on wake kinetic energy and induced drag has been neglected here as the appropriate unsteady corrections are not known. The fluid dynamics resulting from the interaction of linear wingtip trailing vortices with the ground were described by Harvery & Perry (1971), who observed a rebound of the vortex once it reached a minimum distance from the ground. This lifting of the vortex was attributed to the formation of a secondary vortex due to boundary layer separation between the two. Barker & Crow (1977) examined the two-dimensional vortex pair in ground effect, and Boldes & Ferreri (1973), among others, have investigated the behaviour of vortex rings near a wall boundary. The unsteady separation of a wall boundary layer due to its interaction with vortex rings embedded in an impinging jet has been studied by Didden & Ho (1985). These studies give some pointers as to the likely fluid dynamics in this case, and in general, it appears that the vortices do not approach closely enough to the ground for the wake structure to be qualitatively affected by its presence. No substantial secondary vortices or boundary layer separation were apparent near the floor in the wake photographs. The qualitative wake structure reported here is probably not significantly influenced by ground effect although, at some stages of the wing beat cycle, particularly towards the end of the downstroke, the induced velocities behind the wing trailing edge may be.

Recent developments

Since the completion of these experiments, preliminary results reported by Rayner (1986*a*), using this flow visualization technique, indicate that the wake of the bat *Nyctalus noctula* may be composed of closed vortex loops at flight speeds of $4\,m\,s^{-1}$, while the wake structure at higher speeds of $9\,m\,s^{-1}$ was interpreted as a continuous undulating vortex pair, following the pattern observed in the kestrel wake. The apparent occurrence of this type of wake in a different class of animal lends support to the foregoing arguments that such a wake structure should be observable in the wake of many, if not most, flying animals with broadly similar wing beat kinematics. Rayner (1986*a*) then goes on to discuss gait changes with flight speed. It is difficult to infer a distinct gait change (sharp discontinuity in wing beat kinematics in the case of flapping flight) from observations at just two flight speeds, and consequently this distinction has been avoided in this discussion. The observed wake structure of the kestrel in cruising flight is indeed quite different from any previously described but one can only speculate as to how small changes in flight speed might affect the *qualitative* structure. With decreasing flight speed, the strength of cross-stream vortex elements might gradually increase as the circulation around the wing decreases on the upstroke and a correspondingly greater amount of vorticity is shed

into the wake at each end of the downstroke, consistent with the greater angular acceleration of the wing at these stages. With further decrease in flight speed, the limit of the closed vortex loop is approached. If the preceding scenario is both plausible and consistent with the gradual kinematic changes with flight speed measured by ciné film analysis (e.g. Scholey, 1983), it still lacks solid experimental evidence. We therefore concur with the arguments of Brown (1953, 1963) who observed different flight kinematics at different flight speeds but was careful to remain equivocal concerning the possible existence of distinct gait changes with speed.

Rayner (1986*b*) has also outlined a flight model which contains some similarities to that introduced in this paper, based as it is on the same experimental data. There are some differences in the specification of the wake geometry, here fixed by b_1' and b_2', whereas his is based on the semispan b, thus ignoring span efficiency. He also specifies a spanwise circulation distribution which minimizes the wing root bending moment as given by Jones (1980), but which differs little from the elliptical loading distribution assumed here in its effect on the calculation of induced drag. His parameters are fixed to allow calculation of wingbeat amplitude, ϕ, and circulation, Γ, with changing frequency, while the approach here has been to calculate the downstroke ratio, τ, and Γ for a given wing *shape*. The two different formulations exemplify two ways in which knowledge of the simple wake geometry with constant circulation of the wake vortices enables approximate but elementary calculation to be made of the effects of changing wing beat kinematics and geometry, respectively.

Implications for flight models

The implications of these results for aerodynamic or energetic models of bird flight depend on their proposed applications. Clearly, the wake geometry is quite unlike the closed vortex loop model of Rayner (1979*a*,*b*) and the changes in circulation, both across the span and with time, are different. In this respect, the wake geometry adopted by Phlips, East & Pratt (1981) is closer to that described here. Their wake model is split into a far wake consisting of streamwise vortices joined by transverse elements formed at the ends of each wing stroke, and a near wake consisting of the surface traced out by the wings on the current wingstroke with transverse vorticity collected at the wing position at the beginning of the stroke. From lifting line theory, a first-order unsteady spanwise loading distribution on the wing was deduced for a simplified wing beat. The results reported here support this line of investigation and prescription of the wake geometry, which may be readily amended to incorporate refinements such as changing effective span on the upstroke. As far as including a more precise description of the variable wing geometry itself, the relatively low reduced frequencies prevalent in this mode of flight (Ω of the order of 10^{-1} based on the wing chord c, Ω of the order of 1 based on the semispan, b) enable an analytical solution to the unsteady lifting-line problem to be made by considering small perturbations of the linearized boundary conditions. A recent example is the asymptotic analysis by Cheng & Murillo (1984) of an oscillating lifting surface with curved centre line and local wing twist, which yields the surface lift distribution on a smooth planar geometry in small amplitude pitching and heaving motion.

However, the assumption of a wake structure of the type described for the medium-speed flight of the kestrel enables a number of simplifications in the calculation of induced drag and induced power to be made, so that the constant circulation model introduced in the previous discussion might profitably be used for quick estimates of these quantities. The unsteadiness of the wake is accounted for by the accurate description of the wake geometry but the constant circulation on the wings allows a simple quasi-steady estimate for the magnitude of the induced drag. On occasions where an estimate of the induced power requirement at moderate flight speeds, typically around U_{mp} or U_{mr}, is required as a component in the calculation of energy budget of a flying bird, the added complexity of a more rigorous and complete aerodynamic model is not justified by the small improvement in accuracy in estimating one component of the total aerodynamic power requirement, and this approximate calculation should suffice.

The structure of the vortex wake behind a kestrel in medium-speed flight shows considerable differences from the wakes previously described for slow flight. The absence of any significant concentrations of transverse vorticity in the wake implies a constant circulation on the wing and makes calculation of the induced power requirement quite a simple matter. If the wing beat kinematics of the kestrel are taken to be reasonably representative of birds in cruising flight, then their wakes should also be similar and the flight model based on such a wake can be applied to predict the flight power requirement. Ground effect has been neglected in the results reported here, but its effect could be investigated by enforcing a minimum flying height with obstacles of various heights placed before and after the measurement area.

It is a pleasure to thank Dr C. J. Pennycuick for his steady supervision during the course of this research, and for a careful reading of the first version of this paper. Thanks also to colleagues Drs J. M. V. Rayner and K. D. Scholey for helpful advice and discussion. The financial support of the Science and Engineering Research Council is gratefully acknowledged.

REFERENCES

BARKER, S. J. & CROW, S. C. (1977). The motion of two-dimensional vortex pairs in a ground effect. *J. Fluid Mech.* **82**, 657–671.

BATCHELOR, G. K. (1967). *An Introduction to Fluid Dynamics*. Cambridge: Cambridge University Press.

BOLDES, U. & FERRERI, J. C. (1973). Behaviour of vortex rings in the vicinity of a wall. *Phys. Fluids* **16**, 2005–2006.

BROWN, R. H. J. (1953). The flight of birds. II. Wing function in relation to flight speed. *J. exp. Biol.* **25**, 90–103.

BROWN, R. H. J. (1963). The flight of birds. *Biol. Rev.* **38**, 460–489.

CHENG, H. K. & MURILLO, L. E. (1984). Lunate-tail swimming propulsion as a problem of curved lifting line in unsteady flow. Part 1. Asymptotic theory. *J. Fluid Mech.* **143**, 327–350.

DIDDEN, N. & HO, C.-M. (1985). Unsteady separation in a boundary layer produced by an impinging jet. *J. Fluid Mech.* **160**, 235–256.

ELLINGTON, C. P. (1984). The aerodynamics of hovering insect flight. IV. Aerodynamic mechanisms. *Phil. Trans. R. Soc. Ser.* B **305**, 79–113.

HARVERY, J. K. & PERRY, F. J. (1971). Flow field produced by trailing vortices in the vicinity of the ground. *AIAA J.* **9**, 1659–1660.

JONES, R. T. (1980). Wing flapping with minimum energy. *Aero. J.* **84**, 214–217.

KOKSHAYSKY, N. V. (1979). Tracing the wake of a flying bird. *Nature, Lond.* **279**, 146–148.

MCCORMICK, B. W. & PADAKANNAYA, R. (1971). The effect of a drooped wing tip on its trailing vortex system. In *Aircraft Wake Turbulence and its Detection: Proceedings of the Symposium*, Seattle, Washington, pp. 157–169.

MILNE-THOMPSON, L. M. (1966). *Theoretical Aerodynamics*. New York: Dover.

PENNYCUICK, C. J. (1968). Power requirements for horizontal flight in the pigeon (*Columba livia*). *J. exp. Biol.* **49**, 527–555.

PENNYCUICK, C. J. (1975). Mechanics of flight. In *Avian Biology*, vol. 5 (ed. D. S. Farner, J. R. King & K. C. Parkes). London: Academic Press.

PHLIPS, P. J., EAST, R. A. & PRATT, N. H. (1981). An unsteady lifting line theory of flapping wings with application to the forward flight of birds. *J. Fluid Mech.* **112**, 97–125.

RAYNER, J. M. V. (1979*a*). A vortex theory of animal flight. II. The forward flight of birds. *J. Fluid Mech.* **91**, 731–763.

RAYNER, J. M. V. (1979*b*). A new approach to animal flight mechanics. *J. exp. Biol.* **80**, 17–54.

RAYNER, J. M. V. (1986*a*). The mechanics of flapping flight in bats. In *Recent Advances in the Study of Bats* (ed. M. B. Fenton, P. A. Racey & J. M. V. Rayner). Cambridge: Cambridge University Press (in press).

RAYNER, J. M. V. (1986*b*). Vertebrate flapping flight mechanics and aerodynamics, and the evolution of flight in bats. In *Biona Report*, no. 5 (ed. W. Nachtigall) (in press).

SCHOLEY, K. D. (1983). Developments in vertebrate flight: climbing and gliding of mammals and reptiles, and the flapping flight of birds. Ph.D. thesis, University of Bristol.

SPEDDING, G. R. (1986). The wake of a jackdaw (*Corvus monedula*) in slow flight. *J. exp. Biol.* **125**, 287–307.

SPEDDING, G. R. (1987). The wake of a kestrel (*Falco tinnunculus*) in gliding flight. *J. exp. Biol.* **127**, 45–57.

SPEDDING, G. R., RAYNER, J. M. V. & PENNYCUICK, C. J. (1984). Momentum and energy in the wake of a pigeon (*Columba livia*) in slow flight. *J. exp. Biol.* **111**, 81–102.